

# Geophysical Research Letters

## RESEARCH LETTER

10.1029/2020GL087933

### Key Points:

- An ENSO event can activate a subtropical Pacific mechanism to onset another event resulting in a cyclic or multiyear ENSO transition
- Mean SSTs in the cold tongue and warm pool respectively control how easily cyclic and multiyear transitions can occur via this process
- A future warming of the tropical Pacific is projected to reduce (increase) the occurrence of the multiyear (cyclic) ENSO transitions

### Supporting Information:

- Supporting Information S1
- Figure S1
- Figure S2
- Figure S3
- Figure S4
- Figure S5
- Figure S6
- Figure S7
- Figure S8
- Figure S9

### Correspondence to:

J.-Y. Yu,  
jyu@uci.edu

### Citation:

Fang, S.-W., & Yu, J.-Y. (2020). A control of ENSO transition complexity by tropical Pacific mean SSTs through tropical-subtropical interaction. *Geophysical Research Letters*, 47, e2020GL087933. <https://doi.org/10.1029/2020GL087933>

Received 14 MAR 2020

Accepted 30 APR 2020

Accepted article online 10 MAY 2020

## A Control of ENSO Transition Complexity by Tropical Pacific Mean SSTs Through Tropical-Subtropical Interaction

Shih-Wei Fang<sup>1</sup>  and Jin-Yi Yu<sup>1</sup> 

<sup>1</sup>Department of Earth System Science, University of California, Irvine, CA, USA

**Abstract** El Niño–Southern Oscillation (ENSO) transitions from one event to another in complex ways. Using observational analyses and forced atmospheric model experiments, we show that a preceding ENSO event can activate a subtropical Pacific forcing mechanism to trigger another ENSO event during the following year. These tropical-subtropical Pacific interactions result in a cyclic ENSO transition if the two ENSO events are of opposite signs or a multiyear ENSO transition if they are of the same sign. The preceding ENSO event should excite deep convections in the tropical Pacific in order to activate the subtropical Pacific mechanism. This requirement enables mean temperatures in the cold tongue and warm pool to respectively control how easily the cyclic and multiyear transitions can occur. A future warmer tropical Pacific is projected to decrease the frequency of occurrence of multiyear ENSO transitions but increase the occurrence of cyclic ENSO transitions.

**Plain Language Summary** El Niño–Southern Oscillation (ENSO) is one of the strongest climate variation phenomena in Earth's climate system, causing regional climate extremes and massive ecosystem impacts. An ENSO event can transition from one event to another in complex ways. An El Niño (La Niña) event can be preceded by a La Niña (El Niño) event to become a cyclic ENSO, by a neutral event to become an episodic ENSO, or by another El Niño (La Niña) event to become a multiyear ENSO. The complex nature of ENSO transition challenges our understanding of ENSO dynamics and its future responses to greenhouse warming. Here we show, using observational analyses, climate model simulations, and a novel framework focusing specifically on the onset processes of ENSO, that multiyear ENSO events related to the subtropical forcing are projected to decrease and cyclic ENSO events to increase as the climate warms. These changes in ENSO transition complexity are linked to the warming of the tropical Pacific mean state, which is a key factor controlling ENSO transitions through a series of tropical-subtropical interactions.

## 1. Introduction

El Niño–Southern Oscillation (ENSO) is the strongest year-to-year phenomenon in our global climate, causing regional climate extremes and massive ecosystem impacts (Coelho & Goddard, 2009; Donnelly & Woodruff, 2007; McPhaden et al., 2006; Power et al., 2013). ENSO has recently been observed to exhibit a wide range of complex behaviors (Capotondi et al., 2015; Timmermann et al., 2018; Yu et al., 2017) that impede our understanding of its physical dynamics and results in huge uncertainties in projecting its future changes (Amaya, 2019; Cai et al., 2015; Collins et al., 2010; Fedorov et al., 2003; Sohn et al., 2016; Vecchi & Wittenberg, 2010). One aspect of ENSO complexity is related to the ways that ENSO transitions from one event to another (Wang et al., 2019; Yu & Fang, 2018). An El Niño (La Niña) event can be preceded (1) by a La Niña (El Niño) event to become a cyclic ENSO transition, (2) by a neutral event to become an episodic ENSO transition, or (3) by another El Niño (La Niña) event to become a multiyear ENSO transition. Unlike most other studies of ENSO complexity that focus on properties during the peak phase, ENSO transition complexity focuses on ENSO properties during the onset phase.

Whether an ENSO event goes through a cyclic, episodic, or multiyear transition is affected by its onset (or trigger) mechanism (Yu & Fang, 2018)—the process by which the initial ENSO sea surface temperature (SST) anomalies are produced in the equatorial Pacific. Two primary onset mechanisms have been identified by the research community over the past decades (see reviews in Capotondi et al., 2015; Wang et al., 2017; Yang et al., 2018; Yu et al., 2017). The tropical Pacific onset (TP onset) mechanism consists of the

recharge oscillator (Jin, 1997; Wyrtki, 1975) and delayed oscillator (Battisti & Hirst, 1989; Zebiak & Cane, 1987) theories. Together, these theories describe how equatorial surface wind anomalies induced by an ENSO event can deepen or shallow the thermocline in the equatorial eastern Pacific over the following months, and onset another ENSO event with an opposite phase. The TP onset mechanism leads mostly to cyclic ENSO transitions and contributes to reduce ENSO transition complexity (Yu & Fang, 2018), although it should be noted that its asymmetric responses between El Niño and La Niña may allow for some complexity (Hu et al., 2017). In contrast, the subtropical Pacific onset (SP onset) mechanism describes how subtropical Pacific SST anomalies can intrude into the equatorial Pacific to trigger ENSO events (Alexander et al., 2010; Anderson & Perez, 2015; Kao & Yu, 2009; Vimont et al., 2003; Yu et al., 2010). This onset mechanism has been shown to produce all three transition patterns (Yu & Fang, 2018; Figure S1 in the supporting information). Therefore, the SP onset mechanism is a key contributor to ENSO transition complexity and needs to be better understood for projecting future changes in ENSO complexity.

To trigger an ENSO event, the SP onset mechanism is initiated by a decrease or increase in trade winds that extends from off the coast of Baja California to the equatorial central Pacific that respectively warms or cools SSTs underneath. The wind and SST anomalies can prolong for several months through a wind-evaporation-SST feedback (WES; Xie & Philander, 1994) (aka the Pacific meridional mode (PMM) in Chiang and Vimont, 2004, or seasonal footprinting mechanism in Vimont et al., 2003). The initial trade wind variations are often induced by subtropical atmospheric processes (such as the North Pacific oscillation, NPO) that are non-ENSO related (Vimont et al., 2003). Therefore, it is easy to understand why the SP onset mechanism can give rise to episodic ENSO transitions. Less attention has been paid in past studies to the possibility that the SP onset mechanism can also be activated by a preceding ENSO event resulting in either cyclic or multiyear ENSO transitions.

The limited studies on the ENSO-induced SP onset mechanism have found that extreme El Niño events can activate the SP onset mechanism to trigger La Niña events during the following year and result in a cyclic El Niño-to-La Niña transition (Yu & Fang, 2018; Yu & Kim, 2011). Interestingly, the opposite tendency of a cyclic La Niña-to-El Niño transition via the SP onset mechanism seems to occur less frequently (Yu & Fang, 2018). The SP onset mechanism appears to respond asymmetrically to El Niño and La Niña. What is the cause for this asymmetry and how will this asymmetry change in the future as the earth warms? Answers to these questions are important to project future changes in ENSO transition complexity and are the main focus of this study.

## 2. Data Sets and Methods

Monthly mean values of SST, surface wind, geopotential height, precipitation, and sea surface height (SSH) during the period of 1958–2014 were used after they were regridded to a common  $1.5^\circ \times 1^\circ$  longitude-latitude grid covering the tropical Pacific ( $20^\circ\text{S}$  to  $20^\circ\text{N}$ ,  $122^\circ\text{E}$  to  $70^\circ\text{W}$ ). The SST data are the Hadley Center Sea Ice and Sea Surface Temperature data set (Rayner et al., 2003), the surface wind, geopotential height, and precipitation fields are from the National Centers for Environmental Prediction/National Center for Atmospheric Research (Kalnay et al., 1996), and the SSH data are produced by the German contribution of the Estimating the Circulation & Climate of the Ocean (Köhl, 2015). Anomalies are defined as the deviations from the seasonal cycle averaged over the analysis period after removing the linear trend. The same procedures were applied to the simulations (the last 100 years of the preindustrial simulations and the full periods of the historical, RCP4.5 and RCP8.5 simulations) produced by 28 models of the Coupled Model Intercomparison Project (CMIP5) (Taylor et al., 2012; see Extended Data Table S1). Similar results are obtained when a quadratic trend removal is applied (in place of the linear trend removal).

Several indices were used in the analyses. Indices of the SP and TP onset mechanisms were constructed by applying a multivariate empirical orthogonal function (MEOF) analysis to combined SST, wind, and SSH anomalies in the tropical Pacific (Text S1; Xue et al., 2000; Yu & Fang, 2018). These indices are referred to as the SP onset index and the TP onset index. A Niño3.4 index is used to represent the intensity of ENSO events and is defined as the SST anomalies averaged between  $5^\circ\text{S}$  to  $5^\circ\text{N}$  and  $170\text{--}120^\circ\text{W}$ . The equatorial eastern Pacific (EEP) region is defined as the area between  $5^\circ\text{S}$  to  $5^\circ\text{N}$  and  $120\text{--}90^\circ\text{W}$ , whereas the equatorial central Pacific (ECP) region is defined as the area between  $5^\circ\text{S}$  to  $5^\circ\text{N}$  and  $160^\circ\text{E}$  to  $170^\circ\text{W}$ . A series of forced experiments were conducted in this study with an atmospheric general circulation model (AGCM). The designs of these model experiments are described in the supporting information (Text S2).

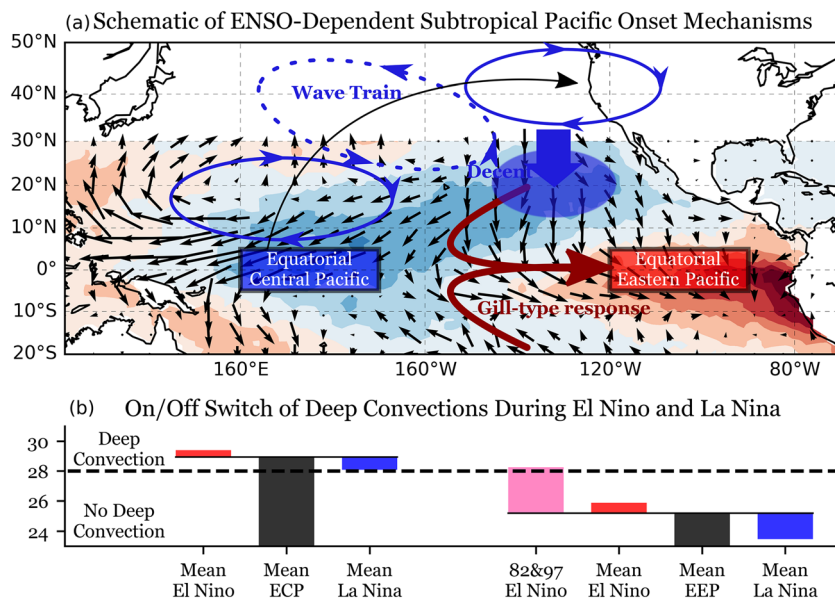


**Figure 1.** (a) Schematic of the processes that enable SST anomalies (color shading) in the equatorial central Pacific (ECP) or equatorial eastern Pacific (EEP) to excite the surface wind anomalies (vectors) associated with the subtropical Pacific onset mechanism via a Gill-type response (brown arrows) and Rossby wave train in the lower troposphere (blue solid and dashed arrows) and the associated descending motions (large blue arrow); (b) the departures of the ECP and EEP SSTs ( $^{\circ}$ C) from the threshold SST value for deep convection ( $28^{\circ}$ C; horizontal thick-dashed line) in their climatological state (horizontal thin-solid lines) and with the values added by the typical SST anomaly values of El Niño (red bars), La Niña (blue bars), and the 1982–1983 and 1997–1998 extreme El Niño events (pink bar).

### 3. Results

We first examine the anomaly pattern associated with the SP onset mechanism by regressing SST and surface wind anomalies onto the SP onset index (Figure 1a). A key feature in the pattern is the overlap of trade wind anomalies with SST anomalies in the northeastern subtropical Pacific. This overlap reflects the subtropical coupled nature of the SP onset mechanism, which is a key to extending the SST anomalies southwestward into the equatorial central Pacific for the ENSO onset. A negative phase of the SP onset mechanism (see Figure 1a) can onset a La Niña event, whereas a positive phase of the SP onset mechanism can onset an El Niño event. As mentioned, the NPO used to be considered to be a key source for the trade wind anomalies. However, Figure 1a indicates that subtropical Pacific trade wind anomalies may also be related to the large SST anomalies in the equatorial eastern Pacific (EEP) and the equatorial central Pacific (ECP).

The pair of anomalous cyclones straddling the equator to the west of the EEP SST anomalies appears to be a Gill-type response (Gill, 1980) to the SST anomalies. The trade wind anomalies over the northeastern subtropical Pacific are associated with the anomalous cyclone to the north. This anomaly structure suggests that the subtropical Pacific trade wind anomalies can be the result of a Gill-type response to the EEP SST anomalies (as illustrated by the red vectors in Figure 1a) (Wang et al., 2000). An El Niño (La Niña) event in the EEP can activate a negative (positive) phase of the SP onset mechanism to trigger a subsequent La Niña (El Niño) event, giving rise to a cyclic ENSO transition. On the other hand, the same trade wind anomalies over the northeastern Pacific can also be linked to the ECP SST anomalies through a wave train pattern connecting the two regions (as illustrated by the blue circles in Figure 1a) (Lyu et al., 2017; Stuecker, 2018). A La Niña (El Niño) event in the ECP can activate a negative (positive) phase of the SP onset mechanism to trigger another La Niña (El Niño) event, giving rise to a multiyear ENSO transition. Therefore, the Gill-type response and the basin-wide wave train enable the SP onset mechanism to produce cyclic ENSO transitions through the EEP region and multiyear ENSO transitions through the ECP region.

In order to excite the Gill-type response and the wave train, ENSO events in the EEP and ECP should induce convective heating anomalies. The threshold value for deep convection is around  $28^{\circ}$ C (Sud et al., 1999; Zhang, 1993), which is confirmed for both the EEP and ECP regions by examining the relationships

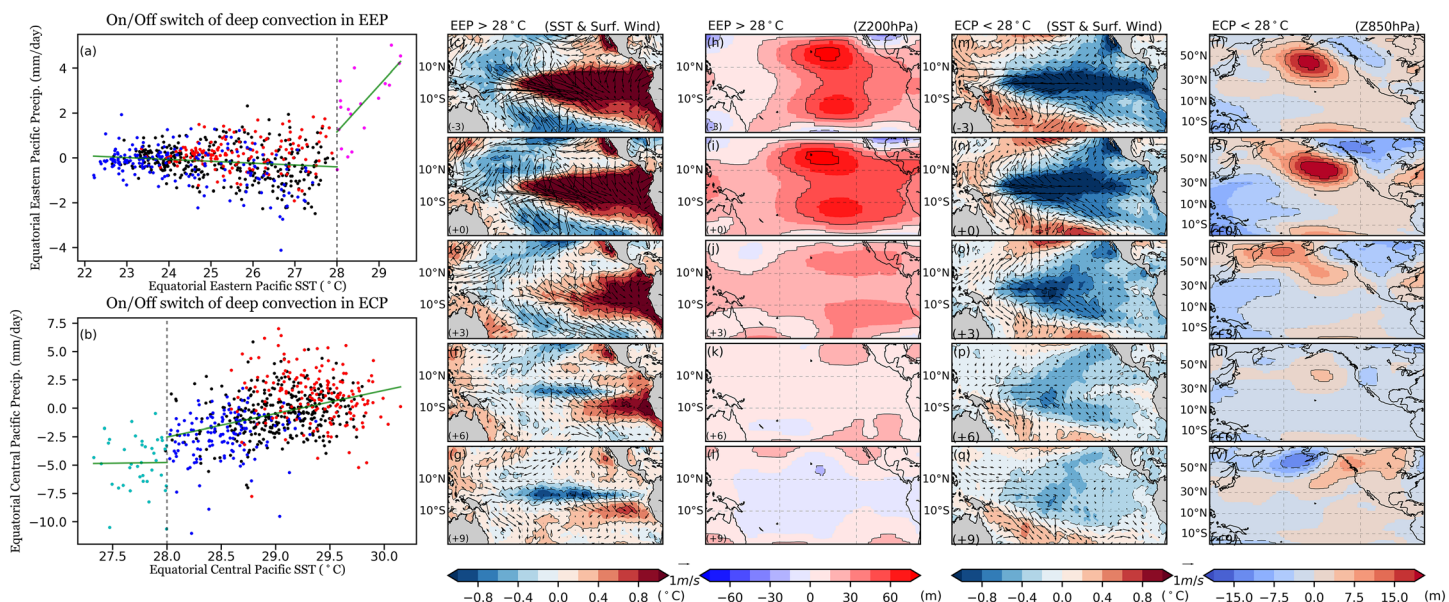


**Figure 2.** Relations between precipitation anomalies and SSTs (a) in the equatorial eastern Pacific (EEP) and (b) the equatorial central Pacific (ECP). Green lines are the linear fits for SSTs greater and less than 28°C. The pink dots are El Niño months when the SST > 28°C; red dots are El Niño months when SST < 28°C; and the blue and light blue dots are the La Niña months when SST > 28°C and SST < 28°C. Evolution of (c–g) SST, surface winds, and (h–l) 200 hPa geopotential heights anomalies composites for the months in which the EEP SST is greater than 28°C at time lags of −3, 0, +3, +6, and +9 months (in the lower left corner of the subpanels). (m–v) The months when ECP SST is lower than 28°C and 850 hPa geopotential heights in the right column.

between precipitation anomalies and SSTs over the regions (Figures 2a and 2b). A composite of all El Niño months when the EEP SSTs are greater than 28°C (the pink dots in Figure 2a) reveals strong evidence of a Gill-type response, which is characterized by a pair of anomalous cyclones in the lower troposphere (Figures 2c–2g) and a pair of anticyclones in the upper troposphere (Figures 2h–2l). An analysis of the time series of the EEP and SP onset indices confirms that a negative SP onset index occurs after the EEP SST index passes the 28°C threshold (Figure S2a). The El Niño-induced anomalous trade winds (and the negative SP onset mechanism) bring anomalous cold water over the subtropical Pacific toward the tropical central Pacific and switch the composite SST anomalies from El Niño to La Niña condition (Figures 2c–2g). In contrast, the Gill-type response is either very weak or absent when we repeat the composite for all El Niño months where the EEP SSTs are lower than 28°C (the red dots in Figure 2a) or with all La Niña months (the blue dots in Figure 2a) (see Figure S3).

Our composite results confirm that only El Niño events that are strong enough to raise EEP SSTs higher than 28°C can activate the SP onset mechanism to produce the cyclic ENSO transition. Since the climatological SST in the EEP (25.19°C) is lower than the 28°C threshold (Figure 1b), it is impossible for La Niña events to induce anomalous convective heating and activate this mechanism. This explains why the SP onset mechanism produces more El Niño-to-La Niña than La Niña-to-El Niño transitions (Yu & Fang, 2018). There are only two such very strong El Niños during the analysis period: the 1982–1983 and 1997–1998 El Niños. We notice that the SP onset index only becomes strongly negative after the EEP SSTs exceed the 28°C during these two extreme events (Figure S2b). In addition, the SP onset indices are stronger than the TP onset indices during these events (lag-0 in Figure S5a). This confirms that only extreme warming in the EEP can enable the SP onset mechanism to dominate the TP onset mechanism and to initiate cooling in the ECP resulting in cyclic transitions (Yu & Kim, 2011). Therefore, the climatological SST in the EEP region determines how easily and what type of cyclic ENSO evolution (i.e., El Niño-to-La Niña or La Niña-to-El Niño) can be produced via the SP onset mechanism. It should be noted that the TP onset mechanism also contributes to the cyclic transitions in these extreme cases.

Over the ECP region, the climatological SST (28.94°C) is just slightly above the 28°C threshold. Therefore, even moderate La Niña events here can shut off deep convections, resulting in large negative convective

heating anomalies (Figure 1b). A composite analysis was performed with the La Niña months that lower the local SSTs to below 28°C. The results indicate that a La Niña event that shuts off deep connection in the ECP region can excite wave train responses that extend into the extratropical lower troposphere (Figures 2r–2v). The wave train includes an anomalous anticyclone off the North American coast that can further induce anomalous descent over the northeastern subtropical Pacific via geostrophic processes (Lyu et al., 2017). The subsidence then enhances the trade winds and initiates a negative phase of the SP onset mechanism (Figure 2b; Figure S7 in Yu & Fang, 2018) to onset another La Niña condition (Figures 2m–2q). The negative values of the SP onset index are confirmed during these events, while the TP onset index follows its own cycle leading to positive values (Figure S5b). Therefore, even moderate La Niña events in the ECP region can result in a multiyear La Niña transition through the SP onset mechanism.

El Niño events in this region can also strengthen deep convection to produce positive convective heating anomalies. However, since most of the central Pacific El Niño (Kao & Yu, 2009; Yu & Kao, 2007) are of weaker SST anomalies (Lee & McPhaden, 2010), the anomalous heating they induce are relatively small. A composite of the El Niño months in the ECP region (Figures S4p–S4t) indicates that the extratropical wave train pattern excited by warm ECP SST anomalies is relatively weaker than that excited by cold ECP SST anomalies (cf. Figures S4q and S2s). Also, the evolution of the composite SST anomalies does not show multiyear El Niño transitions (Figures S4k–S4o). A similar result was obtained in the composite analysis of weak La Niña events that do not lower ECP SSTs to below 28°C (Figures S4a–S4j).

Our composite analyses indicate that La Niña events in the ECP are more effective than El Niño events in giving rise to multiyear ENSO transitions through the SP onset mechanism. This explains why the SP onset mechanism produces more multiyear La Niña transitions than multiyear El Niño transitions (Yu & Fang, 2018). Therefore, the climatological SST in the ECP region determine how easily and what type of multiyear transitions (i.e., multiyear La Niña or multiyear El Niño) can be produced via the SP onset mechanism.

The processes described above were further confirmed by a series of forced AGCM experiments conducted with the Community Earth System Model version 2 (CESM2) (see Text S2). In the experiments, Gaussian shaped SST anomalies were prescribed and added onto the climatological SSTs in either the ECP or EEP region with an amplitude varied from  $-4^{\circ}\text{C}$  to  $+4^{\circ}\text{C}$ . The EEP experiments confirm that the SST anomalies have to be large enough ( $+4^{\circ}\text{C}$ ) to raise EEP SSTs above the 28°C threshold to excite deep convection (Figure S6a), induce the Gill-type responses, and enhance the surface trade winds over the northeastern subtropical Pacific for activating a negative SP onset mechanism (Figure S6c). No such response was found in the other EEP experiments (Figures S6a and S6b). The ECP experiments confirm that large and negative deep convection anomalies can be induced by moderate cold ( $-1^{\circ}\text{C}$  SST) anomalies in the region, which can then excite a wave train response in the extratropical atmosphere and enhance the trade winds to activate a negative SP onset mechanism (Figure S7). In contrast, the wave train response is weaker in the  $+1^{\circ}\text{C}$  SST experiment (Figure S7c). In addition, the weak wave train in this experiment emanates from a more eastern part of the ECP region (compared to the  $-1^{\circ}\text{C}$  experiment) and results in a surface wind response that is away from the trade wind region.

Tropical Pacific mean SSTs are projected to increase in the future (Kirtman et al., 2013; Levitus et al., 2009; Meehl et al., 2006). The multimodel mean (MMM) of the simulations using 28 CMIP5 models (Table S1) show that mean SSTs in the EEP are projected to reach 28°C around 2100 (2060) under the RCP4.5 (RCP8.5) scenario (Figure 3a). This tendency should enable El Niño events of any intensity to induce anomalous deep convection in the EEP, activate the negative phase of the SP onset mechanism, and give rise to cyclic El Niño-to-La Niña transitions. Conversely, as the mean temperatures increase and exceed the threshold, La Niña events in the EEP will be able to shut off deep convection and lead to a subsequent El Niño event via a positive SP onset mechanism. The latter process should give rise to cyclic La Niña-to-El Niño transitions. As a result, cyclic ENSO transitions (i.e., both El Niño-to-La Niña and La Niña-to-El Niño) should occur more frequently via the SP onset mechanism in the future. On the other hand, the projected temperature increases in the ECP region (Figure 2b) will make it harder for La Niña events to reduce ECP SSTs below 28°C and to activate a negative SP onset mechanism in the region. This should result in fewer multiyear La Niña transitions via the SP onset mechanism in the future. In other words, the warmer tropical Pacific in the future is expected to increase the dominance of the cyclic ENSO transition via the SP onset mechanism and to reduce the occurrence of the multiyear ENSO transition.

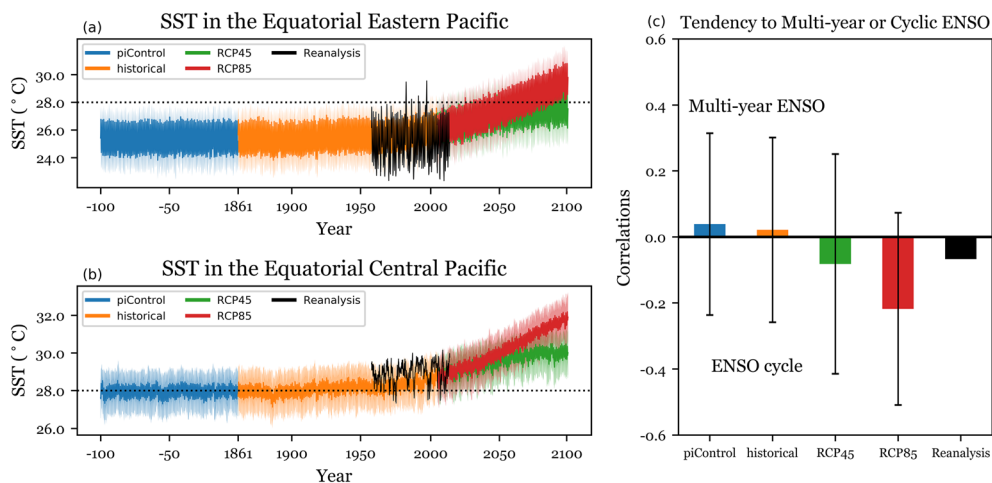


**Figure 3.** CMIP5 model projected SSTs in (a) the equatorial eastern Pacific and (b) equatorial central Pacific from preindustrial times to 2100 and (c) the changes in the tendency of the multiyear ENSO versus cyclic ENSO. In (a) and (b), the thick lines are the multimodel means and the thin lines are the spreads of the projected SSTs from preindustrial (blue) and historical (orange) to RCP4.5 (green) and RCP8.5 (red) calculated from the 28 models. The black solid lines are based on the reanalysis data. In (c), the tendency is represented by the strongest correlation coefficient when the Niño3.4 index leads the SP onset index by 1 to 6 months. The multimodel means of the preindustrial (blue), historical (orange), RCP4.5 (green), and RCP8.5 (red) simulations are shown, and the reanalysis is in black. Solid bars are the standard deviations of the model tendency.

It has been suggested that the threshold value for tropical convection may change as the climate warms (Johnson & Xie, 2010), which can affect our argument above. To assess this possible impact, we examine the relationships between ENSO SST anomalies and precipitation anomalies over the EEP and ECP regions in the preindustrial, historical, RCP4.5, and RCP8.5 simulations (Figure S8). We find that, in the EEP region (Figures S8a–S8d), the same magnitudes of El Niño SST anomalies induce larger precipitation (i.e., deep convection) anomalies as the region warms (from preindustrial to RCP8.5 simulations). On the other hand, the La Niña events in the ECP region (Figures S8e–S8h) require larger negative anomalies to turn off the deep convection (i.e., reduce the precipitation to 0) in the RCP8.5 simulation than in the preindustrial simulation. These results indicate that, even if the 28°C threshold may not remain unchanged or other factors may appear to moderate regional deep convection (Back & Bretherton, 2009; Sabin et al., 2013), a warmer mean state of the tropical Pacific enable El Niño events to turn on deep convections more easily over the EEP region but make La Niña events less easily to turn off deep convections over the ECP region.

We further examine if the ENSO transition complexity related to the SP onset mechanism changes from the preindustrial to RCP simulations. Figure 3c shows the MMM of the strongest lead correlation of the Niño3.4 index with the SP onset index. A positive correlation implies a multiyear transition via the SP onset mechanism, since an El Niño (La Niña) event leads to a positive (negative) phase of the SP onset mechanism and should later develop into another El Niño (La Niña) event. Conversely, a negative correlation implies a cyclic transition. A weak negative value is found in the reanalysis product, which is consistent with the fact that both multiyear ENSO and cyclic ENSO events are observed (Yu & Fang, 2018). In the CMIP5 simulations, the MMM values change from weakly positive in the preindustrial and historical simulations to strong negatives in the RCP4.5 and RCP8.5 simulations. This tendency indicates that, as the Pacific Ocean warms, the SP onset mechanism tends to change from a preference for generating multiyear transitions to a preference for cyclic transitions. This future change of ENSO transition complexity is consistent with our projection based on the control of the tropical Pacific mean state on the SP onset mechanism.

Consistent results can be found by examining the transition patterns of SST anomalies composited for large values of the SP onset index (Figure 4). Both the positive and negative phases of the SP onset mechanism produce a transition pattern that changes from being dominated by multiyear ENSO transitions in present-day simulations to being dominated by cyclic ENSO transitions in the RCP simulations. Furthermore, in the preindustrial and historical simulations, the simulated mean ECP SSTs are colder

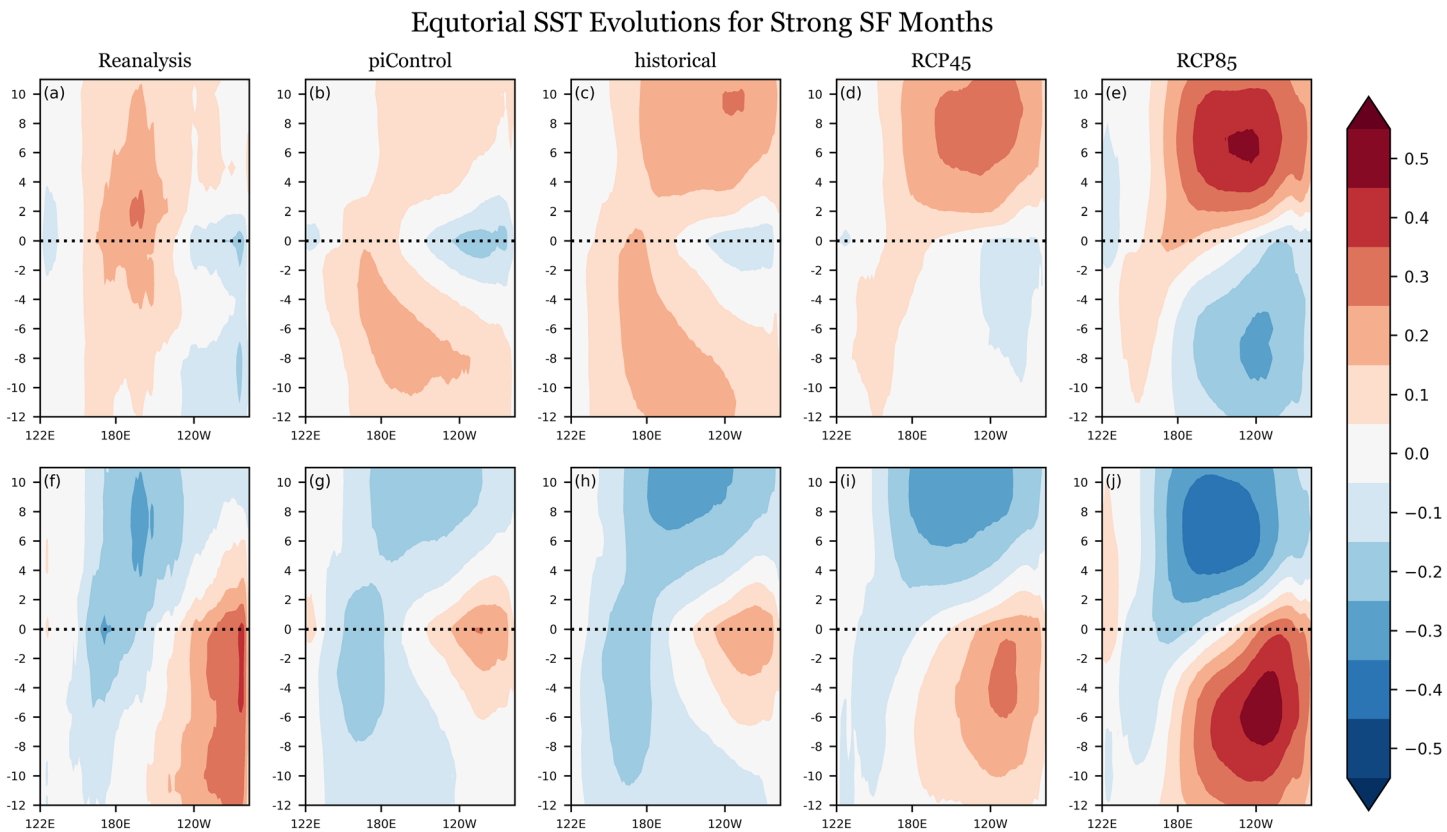


**Figure 4.** Evolution of equatorial SST anomalies associated with the SP onset mechanism. The values shown are the SST anomalies compositized for strong events of the positive (upper panels) and negative (lower panels) phases of the SP onset mechanism, which were identified respectively as the months in which the SP onset index is larger than 0.7 times its standard deviation or lower than  $-0.7$  times its standard deviation. The evolution extends from 12 months before to 12 months after the events and is calculated from the reanalysis (first column) and the multimodel means for the preindustrial (second column), historical (third column), RCP4.5 (fourth column), and RCP8.5 runs (fifth column). The SSTs are normalized by the standard deviation of their modeled Niño3.4 index before the composites are formed and the color bar for the reanalysis panel is 2 times larger than those of the other panels (shown on the right in  $^{\circ}\text{C}$ ).

(around  $28^{\circ}\text{C}$ ; see Figure 3b) than the reanalysis SSTs ( $28.94^{\circ}\text{C}$ ). Therefore, both El Niño and La Niña can enhance or suppress deep convections to give rise to multiyear events. The models with colder ECP SSTs tend to simulate more multiyear El Niños, while the models with warmer ECP SSTs have more multiyear La Niñas as the observations (Figure S9). This CMIP5 model deficiency in simulating too frequent multiyear El Niños in the present-day climate further supports the notion that mean SSTs in the ECP region control the frequency of occurrence of multiyear ENSO transitions.

#### 4. Summary and Discussion

We have, in this study, shown that the tropical Pacific mean SSTs control the ENSO transition complexity produced by the SP onset mechanism. Since the SP onset mechanism is a key source of the transition complexity, our finding offers a way to use tropical Pacific mean states to assess future or past ENSO transition complexities. More interestingly, we find the mean SSTs in different parts of the equatorial Pacific matter for different ENSO transition patterns. The mean SSTs in the EEP region affects how frequently cyclic ENSO transitions can occur, whereas the mean SSTs in the ECP affect how frequently multiyear transitions can occur. We find these relationships are useful to link CMIP5 model deficiencies in simulating ENSO transition complexity and tropical Pacific mean state simulations. Finally, the control of the tropical mean state can also explain why the SP onset mechanism responds differently to El Niño and La Niña, which is a key source of El Niño-La Niña asymmetries that has not yet been fully explored nor understood.

## Acknowledgments

We thank two anonymous reviewers for their valuable comments. This research is supported by the National Science Foundation's (NSF) Climate & Large-scale Dynamics Program under Grant AGS-1833075. The CESM project is supported primarily by the NSF. We acknowledge the World Climate Research Programme's Working Group on Coupled Modeling, which is responsible for CMIP, and we thank the climate modeling groups (listed in Extended Data Table S1) for producing and making available their model output. For CMIP the U.S. Department of Energy's Program for Climate Model Diagnosis and Intercomparison provides coordinating support and led development of software infrastructure in partnership with the Global Organization for Earth System Science Portals. The analyses were performed using Python. Model data used in this study were obtained from the CMIP5 international archive (<https://esgf-node.llnl.gov/projects/cmip5/>). The SST data of HadISST were downloaded from (<http://www.metoffice.gov.uk/hadobs/hadisst/data/download.html>). The wind, precipitation, and geopotential height fields of NCAR Reanalysis were from NOAA (<https://www.esrl.noaa.gov/psd/>). The SSH data sets of GECCO2 were downloaded from the Integrated Climate Data Center (<http://icdc.cen.uni-hamburg.de/projekte/easy-init/easy-init-ocean.html>).

## References

- Alexander, M. A., Vimont, D. J., Chang, P., & Scott, J. D. (2010). The impact of extratropical atmospheric variability on ENSO: Testing the seasonal footprinting mechanism using coupled model experiments. *Journal of Climate*, 23(11), 2885–2901. <https://doi.org/10.1175/2010JCLI3205.1>
- Amaya, D. J. (2019). The Pacific meridional mode and ENSO: A review. *Current Climate Change Reports*, 1–12.
- Anderson, B. T., & Perez, R. C. (2015). ENSO and non-ENSO induced charging and discharging of the equatorial Pacific. *Climate Dynamics*, 45(9–10), 2309–2327. <https://doi.org/10.1007/s00382-015-2472-x>
- Back, L. E., & Bretherton, C. S. (2009). On the relationship between SST gradients, boundary layer winds, and convergence over the tropical oceans. *Journal of Climate*, 22(15), 4182–4196. <https://doi.org/10.1175/2009JCLI2392.1>
- Battisti, D. S., & Hirst, A. C. (1989). Interannual variability in a tropical atmosphere–ocean model: Influence of the basic state, ocean geometry and nonlinearity. *Journal of the Atmospheric Sciences*, 46(12), 1687–1712. [https://doi.org/10.1175/1520-0469\(1989\)046%31687:IVIATA%3E2.0.CO;2](https://doi.org/10.1175/1520-0469(1989)046%31687:IVIATA%3E2.0.CO;2)
- Cai, W., Santoso, A., Wang, G., Yeh, S. W., An, S. I., Cobb, K. M., et al. (2015). ENSO and greenhouse warming. *Nature Climate Change*, 5(9), 849–859. <https://doi.org/10.1038/nclimate2743>
- Capotondi, A., Wittenberg, A. T., Newman, M., Di Lorenzo, E., Yu, J. Y., Braconnot, P., et al. (2015). Understanding ENSO diversity. *Bulletin of the American Meteorological Society*, 96(6), 921–938. <https://doi.org/10.1175/BAMS-D-13-00117.1>
- Chiang, J. C., & Vimont, D. J. (2004). Analogous Pacific and Atlantic meridional modes of tropical atmosphere–ocean variability. *Journal of Climate*, 17(21), 4143–4158. <https://doi.org/10.1175/JCLI4953.1>
- Coelho, C. A., & Goddard, L. (2009). El Niño-induced tropical droughts in climate change projections. *Journal of Climate*, 22(23), 6456–6476. <https://doi.org/10.1175/2009JCLI3185.1>
- Collins, M., An, S. I., Cai, W., Ganachaud, A., Guilyardi, E., Jin, F. F., et al. (2010). The impact of global warming on the tropical Pacific Ocean and El Niño. *Nature Geoscience*, 3(6), 391–397. <https://doi.org/10.1038/ngeo868>
- Donnelly, J. P., & Woodruff, J. D. (2007). Intense hurricane activity over the past 5,000 years controlled by El Niño and the West African monsoon. *Nature*, 447(7143), 465–468. <https://doi.org/10.1038/nature05834>
- Fedorov, A. V., Harper, S. L., Philander, S. G., Winter, B., & Wittenberg, A. (2003). How predictable is El Niño? *Bulletin of the American Meteorological Society*, 84(7), 911–920. <https://doi.org/10.1175/BAMS-84-7-911>
- Gill, A. E. (1980). Some simple solutions for heat-induced tropical circulation. *Quarterly Journal of the Royal Meteorological Society*, 106(449), 447–462. <https://doi.org/10.1002/qj.49710644905>
- Hu, Z. Z., Kumar, A., Huang, B., Zhu, J., Zhang, R. H., & Jin, F. F. (2017). Asymmetric evolution of El Niño and La Niña: The recharge/discharge processes and role of the off-equatorial sea surface height anomaly. *Climate Dynamics*, 49(7–8), 2737–2748. <https://doi.org/10.1007/s00382-016-3498-4>
- Jin, F. F. (1997). An equatorial ocean recharge paradigm for ENSO. Part I: Conceptual model. *Journal of the Atmospheric Sciences*, 54(7), 811–829. [https://doi.org/10.1175/1520-0469\(1997\)054%30811:AEORPF%3E2.0.CO;2](https://doi.org/10.1175/1520-0469(1997)054%30811:AEORPF%3E2.0.CO;2)
- Johnson, N. C., & Xie, S. P. (2010). Changes in the sea surface temperature threshold for tropical convection. *Nature Geoscience*, 3(12), 842–845. <https://doi.org/10.1038/ngeo1008>
- Kalnay, E., Kanamitsu, M., Kistler, R., Collins, W., Deaven, D., Gandin, L., et al. (1996). The NCEP/NCAR 40-year reanalysis project. *Bulletin of the American Meteorological Society*, 77(3), 437–471. [https://doi.org/10.1175/1520-0477\(1996\)077%30437:TNYRP%3E2.0.CO;2](https://doi.org/10.1175/1520-0477(1996)077%30437:TNYRP%3E2.0.CO;2)
- Kao, H. Y., & Yu, J. Y. (2009). Contrasting eastern-Pacific and central-Pacific types of ENSO. *Journal of Climate*, 22(3), 615–632. <https://doi.org/10.1175/2008JCLI2309.1>
- Kirtman, B., Power, S. B., Adedoyin, A. J., Boer, G. J., Bojariu, R., Camilloni, I., et al. (2013). Near-term climate change: Projections and predictability. In IPCC (Ed.), *Climate change 2013: The physical science basis. IPCC Working Group I Contribution to AR5* (Chap. 11). Cambridge: Cambridge University Press.
- Köhl, A. (2015). Evaluation of the GECCO2 ocean synthesis: Transports of volume, heat and freshwater in the Atlantic. *Quarterly Journal of the Royal Meteorological Society*, 141(686), 166–181. <https://doi.org/10.1002/qj.2347>
- Lee, T., & McPhaden, M. J. (2010). Increasing intensity of El Niño in the central-equatorial Pacific. *Geophysical Research Letters*, 37(14). <https://doi.org/10.1029/2010GL044007>
- Levitus, S., Antonov, J. I., Boyer, T. P., Locarnini, R. A., Garcia, H. E., & Mishonov, A. V. (2009). Global ocean heat content 1955–2008 in light of recently revealed instrumentation problems. *Geophysical Research Letters*, 36(7). <https://doi.org/10.1029/2008GL037155>
- Lyu, K., Yu, J. Y., & Paek, H. (2017). The influences of the Atlantic multidecadal oscillation on the mean strength of the North Pacific subtropical high during boreal winter. *Journal of Climate*, 30(1), 411–426. <https://doi.org/10.1175/JCLI-D-16-0525.1>
- McPhaden, M. J., Zebiak, S. E., & Glantz, M. H. (2006). ENSO as an integrating concept in earth science. *Science*, 314(5806), 1740–1745.
- Meehl, G. A., Washington, W. M., Santer, B. D., Collins, W. D., Arblaster, J. M., Hu, A., et al. (2006). Climate change projections for the twenty-first century and climate change commitment in the CCSM3. *Journal of Climate*, 19(11), 2597–2616. <https://doi.org/10.1175/JCLI3746.1>
- Power, S., Delage, F., Chung, C., Kociuba, G., & Keay, K. (2013). Robust twenty-first-century projections of El Niño and related precipitation variability. *Nature*, 502(7472), 541–545. <https://doi.org/10.1038/nature12580>
- Rayner, N. A., Parker, D. E., Horton, E. B., Folland, C. K., Alexander, L. V., Rowell, D. P., et al. (2003). Global analyses of sea surface temperature, sea ice, and night marine air temperature since the late nineteenth century. *Journal of Geophysical Research*, 108(D14), 4407. <https://doi.org/10.1029/2002JD002670>
- Sabin, T. P., Babu, C. A., & Joseph, P. V. (2013). SST–convection relation over tropical oceans. *International Journal of Climatology*, 33(6), 1424–1435. <https://doi.org/10.1002/joc.3522>
- Sohn, S. J., Tam, C. Y., & Jeong, H. I. (2016). How do the strength and type of ENSO affect SST predictability in coupled models. *Scientific Reports*, 6(1), 33,790. <https://doi.org/10.1038/srep33790>
- Stuecker, M. F. (2018). Revisiting the Pacific meridional mode. *Scientific Reports*, 8(1), 3216. <https://doi.org/10.1038/s41598-018-21537-0>
- Sud, Y. C., Walker, G. K., & Lau, K. M. (1999). Mechanisms regulating sea-surface temperatures and deep convection in the tropics. *Geophysical Research Letters*, 26(8), 1019–1022. <https://doi.org/10.1029/1999GL900197>
- Taylor, K. E., Stouffer, R. J., & Meehl, G. A. (2012). An overview of CMIP5 and the experiment design. *Bulletin of the American Meteorological Society*, 93(4), 485–498. <https://doi.org/10.1175/BAMS-D-11-00094.1>
- Timmermann, A., An, S. I., Kug, J. S., Jin, F. F., Cai, W., Capotondi, A., et al. (2018). El Niño–Southern Oscillation complexity. *Nature*, 559(7715), 535–545. <https://doi.org/10.1038/s41586-018-0252-6>

- Vecchi, G. A., & Wittenberg, A. T. (2010). El Niño and our future climate: Where do we stand? *Wiley Interdisciplinary Reviews: Climate Change*, 1(2), 260–270.
- Vimont, D. J., Wallace, J. M., & Battisti, D. S. (2003). The seasonal footprinting mechanism in the Pacific: Implications for ENSO. *Journal of Climate*, 16(16), 2668–2675. [https://doi.org/10.1175/1520-0442\(2003\)016%32668:TSFMIT%3E2.0.CO;2](https://doi.org/10.1175/1520-0442(2003)016%32668:TSFMIT%3E2.0.CO;2)
- Wang, B., Luo, X., Yang, Y. M., Sun, W., Cane, M. A., Cai, W., et al. (2019). Historical change of El Niño properties sheds light on future changes of extreme El Niño. *Proceedings of the National Academy of Sciences*, 116(45), 22512–22517. <https://doi.org/10.1073/pnas.1911130116>
- Wang, B., Wu, R., & Fu, X. (2000). Pacific–East Asian teleconnection: How does ENSO affect East Asian climate? *Journal of Climate*, 13(9), 1517–1536. [https://doi.org/10.1175/1520-0442\(2000\)013%31517:PEATHD%3E2.0.CO;2](https://doi.org/10.1175/1520-0442(2000)013%31517:PEATHD%3E2.0.CO;2)
- Wang, C., Deser, C., Yu, J. Y., DiNezio, P., & Clement, A. (2017). El Niño and Southern Oscillation (ENSO): A review. In *Coral reefs of the eastern tropical Pacific*, (pp. 85–106). Netherlands: Springer.
- Wyrtki, K. (1975). El Niño—The dynamic response of the equatorial Pacific Ocean to atmospheric forcing. *Journal of Physical Oceanography*, 5(4), 572–584. [https://doi.org/10.1175/1520-0485\(1975\)005%30572:ENTDRO%3E2.0.CO;2](https://doi.org/10.1175/1520-0485(1975)005%30572:ENTDRO%3E2.0.CO;2)
- Xie, S. P., & Philander, S. G. H. (1994). A coupled ocean-atmosphere model of relevance to the ITCZ in the eastern Pacific. *Tellus A*, 46(4), 340–350. <https://doi.org/10.3402/tellusa.v46i4.15484>
- Xue, Y., Leetmaa, A., & Ji, M. (2000). ENSO prediction with Markov models: The impact of sea level. *Journal of Climate*, 13(4), 849–871. [https://doi.org/10.1175/1520-0442\(2000\)013%30849:EPWMMT%3E2.0.CO;2](https://doi.org/10.1175/1520-0442(2000)013%30849:EPWMMT%3E2.0.CO;2)
- Yang, S., Li, Z., Yu, J. Y., Hu, X., Dong, W., & He, S. (2018). El Niño–Southern Oscillation and its impact in the changing climate. *National Science Review*, 5(6), 840–857. <https://doi.org/10.1093/nsr/nwy046>
- Yu, J. Y., & Fang, S. W. (2018). The distinct contributions of the seasonal footprinting and charged-discharged mechanisms to ENSO complexity. *Geophysical Research Letters*, 45(13), 6611–6618. <https://doi.org/10.1029/2018GL077664>
- Yu, J. Y., & Kao, H. Y. (2007). Decadal changes of ENSO persistence barrier in SST and ocean heat content indices: 1958–2001. *Journal of Geophysical Research*, 112, D13106. <https://doi.org/10.1029/2006JD007654>
- Yu, J. Y., Kao, H. Y., & Lee, T. (2010). Subtropics-related interannual sea surface temperature variability in the central equatorial Pacific. *Journal of Climate*, 23(11), 2869–2884. <https://doi.org/10.1175/2010JCLI3171.1>
- Yu, J. Y., & Kim, S. T. (2011). Relationships between extratropical sea level pressure variations and the central Pacific and eastern Pacific types of ENSO. *Journal of Climate*, 24(3), 708–720. <https://doi.org/10.1175/2010JCLI3688.1>
- Yu, J. Y., Wang, X., Yang, S., Paek, H., & Chen, M. (2017). The changing El Niño–Southern Oscillation and associated climate extremes. In S.-Y. Wang, J.-H. Yoon, C. Funk, & R. Gillies (Eds.), *Climate Extremes: Patterns and Mechanisms* (pp. 1–38). Hoboken, NJ, USA: John Wiley & Sons, Inc. <https://doi.org/10.1002/9781119068020.ch1>
- Zebiak, S. E., & Cane, M. A. (1987). A model El Niño–Southern Oscillation. *Monthly Weather Review*, 115(10), 2262–2278. [https://doi.org/10.1175/1520-0493\(1987\)115%32262:AMENO%3E2.0.CO;2](https://doi.org/10.1175/1520-0493(1987)115%32262:AMENO%3E2.0.CO;2)
- Zhang, C. (1993). Large-scale variability of atmospheric deep convection in relation to sea surface temperature in the tropics. *Journal of Climate*, 6(10), 1898–1913. [https://doi.org/10.1175/1520-0442\(1993\)006%31898:LSVOAD%3E2.0.CO;2](https://doi.org/10.1175/1520-0442(1993)006%31898:LSVOAD%3E2.0.CO;2)



1

2                   *Geophysical Research Letters*

3

Supporting Information for

4

**A Control of ENSO Transition Complexity by Tropical Pacific Mean SSTs through  
Tropical-Subtropical Interactions**

6

Shih-Wei Fang and Jin-Yi Yu

7

Department of Earth System Science, University of California, Irvine, CA, USA

8

9

10   **Contents of this file**

11       Texts S1 to S2

12       Figures S1 to S9

13       Table S1

14

15 **Text S1. Multi-variate empirical orthogonal function analyses**

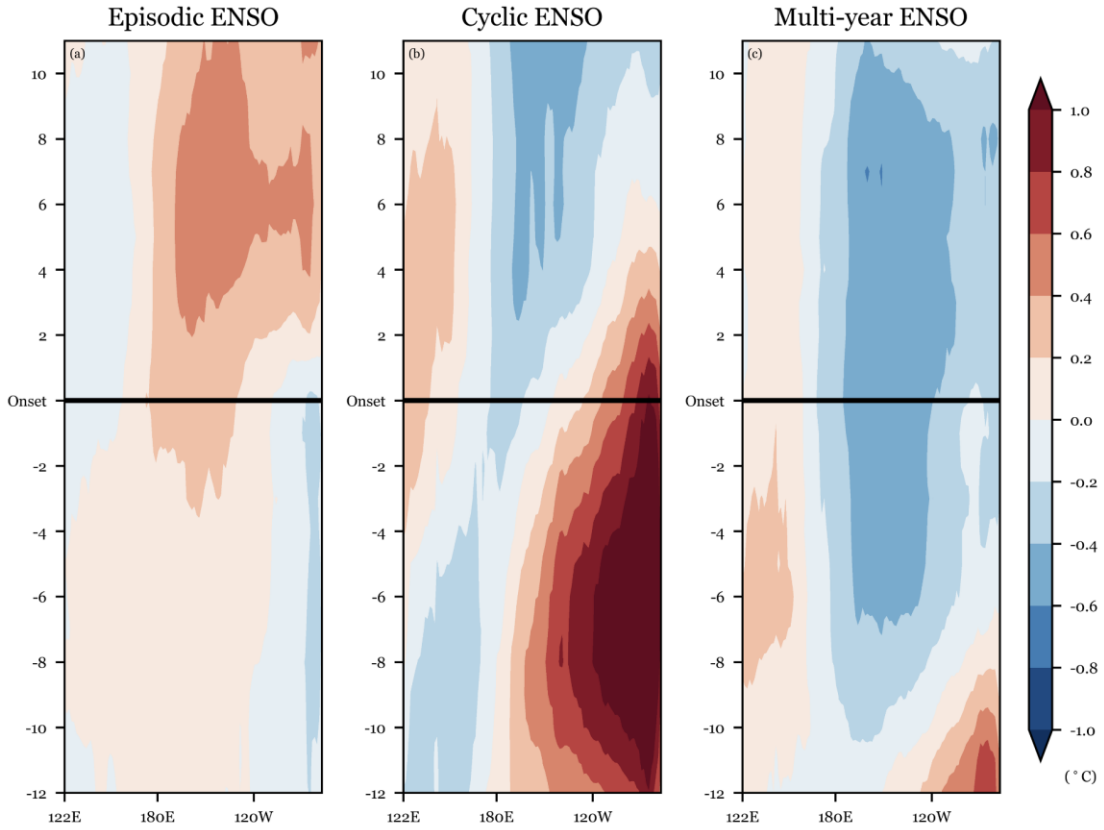
16 Multi-variate empirical orthogonal function (MEOF) analysis is a statistical  
17 method that captures the coupling between multiple variables. In this study, we applied  
18 the MEOF analysis to combined SST, surface wind, and SSH anomalies within the  
19 tropical Pacific over the period of 1958-2014 as in Yu and Fang (2018). Following Xue et  
20 al. (2000), MEOF analysis was performed via two separated empirical orthogonal  
21 function (EOF) analyses. The first is a spatial EOF analysis that was applied to sea  
22 surface temperatures, surface winds, and sea surface heights individually. The three sets  
23 of principal components obtained were then normalized and combined for use in the  
24 second temporal EOF analysis. The leading modes obtained from the temporal EOF  
25 analysis were referred to as the leading MEOF modes. The second leading mode is the  
26 subtropical onset (SP-onset) index in the observation and the tropical onset (TP-onset)  
27 index is the third leading mode. The same MEOF analysis was applied to the last hundred  
28 years of pre-industrial simulations from the fifth phase of the Coupled Model  
29 Intercomparison Project (CMIP5) model simulations and the SP-onset index is identified  
30 following Yu and Fang (2018).

31

32      **Text S2. Forced atmospheric model experiments**

33      We conducted a series of 4-members forced atmospheric model experiments to  
34      examine whether anomalous warming and cooling in the equatorial eastern Pacific (EEP)  
35      and equatorial central Pacific (ECP) regions can excite the surface wind anomaly pattern  
36      associated with the SP-onset mechanism. The model used is the Community Atmosphere  
37      Model version 6 (CAM6) from the Community Earth System Model version 2 (CESM2).  
38      Specifically, the F2000climo component set of CESM2 with the f19\_f19\_mg17  
39      resolution was used, which means that the standalone CAM6 was run with prescribed  
40      seasonal cycles (averaged over 1995-2005) of SSTs and sea-ice extents in the common  
41      1.9x2.5 grid and gx1v7 oceanic resolution for the experiments. The control run is a 7-  
42      year simulation with this default model configuration, from which the November  
43      conditions of the third year were used as the initial conditions for the experiments. The  
44      experiments were integrated from the November initial condition for another three  
45      months with warming or cooling added separately to the EEP or ECP region.

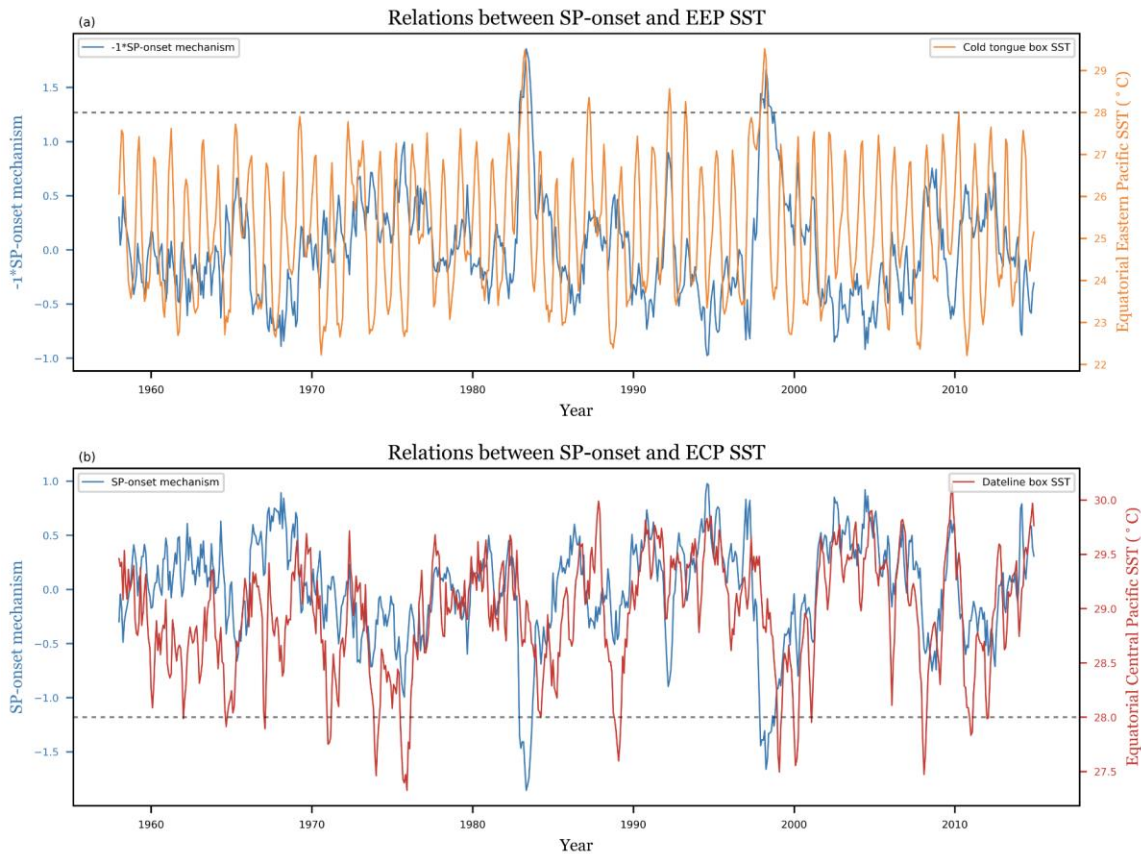
46      In the experiments, we added Gaussian shaped SST anomalies in the EEP or ECP  
47      to the climatological SSTs to study the atmospheric responses. The Gaussian forcing has  
48      a half-width of 45 degrees in longitude and 10 degrees in latitude and is centered at  
49      (175°E, 0°N) when applied to the ECP and at (105°W, 0°N) when applied to the EEP.  
50      The forcing was applied throughout the three months from November to January and the  
51      maximum amplitude of the anomalies was as follows: -4, -3, -2, -1, +1, +2, +3, and +4°C  
52      in each set of EEP and ECP experiments. These different SST amplitudes were designed  
53      to mimic the distinct amplitudes of El Niño and La Niña.



55

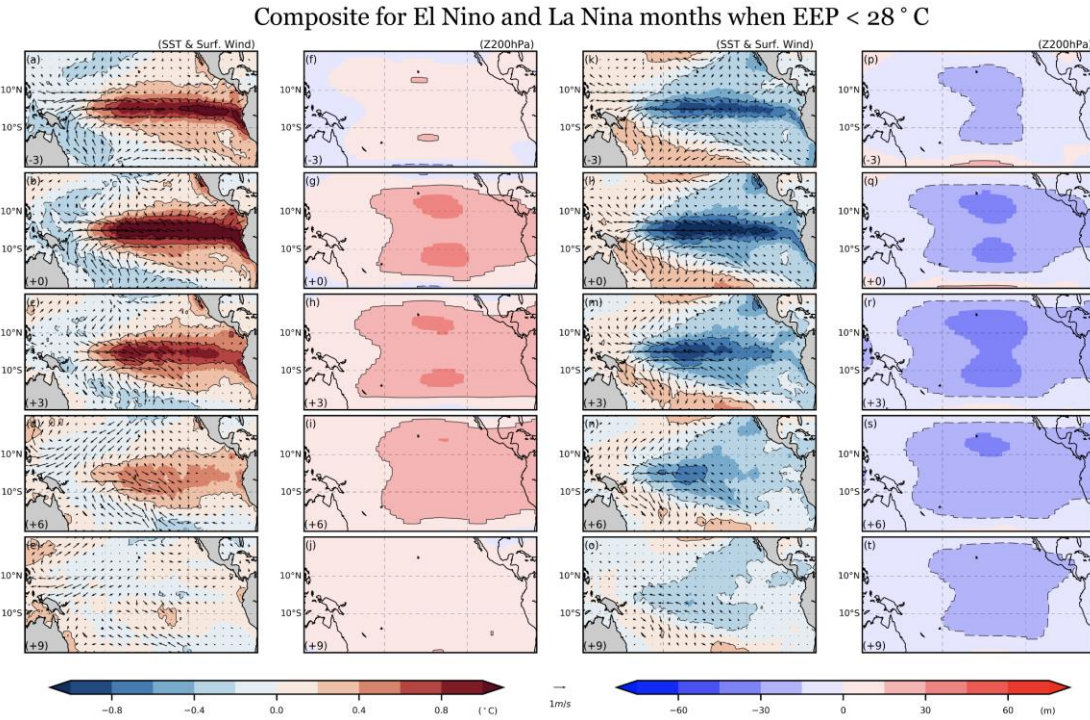
56 **Figure S1.** Evolution of equatorial SST anomalies during the three ENSO transition  
 57 types associated with the subtropical Pacific onset mechanism. a, Equatorial SST  
 58 anomalies composited from observed episodic El Niño events during 1958-2014 from 12  
 59 months before to 12 months after the onset month of El Niño. b, same as a but  
 60 composited from cyclic ENSO events (specifically El Niño-to-La Niña) months. c, same  
 61 as a but composited from multi-year La Niña months. The onset month is defined as the  
 62 month when the SP-onset index becomes larger than 0.7 times its standard deviation.

63



64

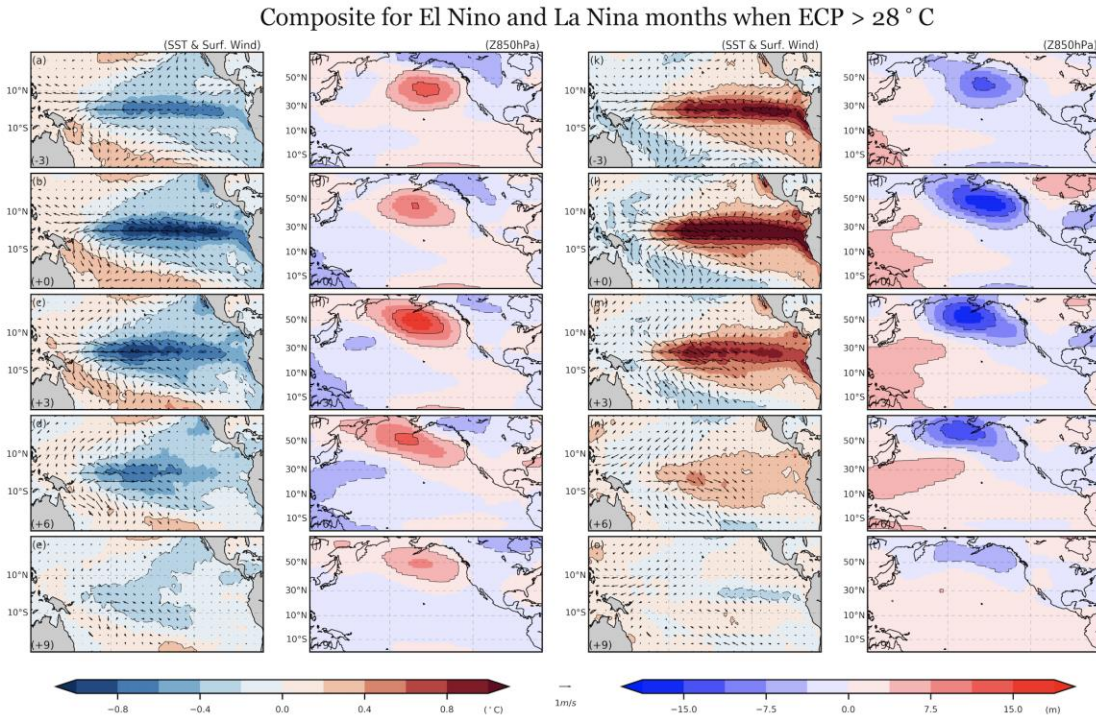
65 **Figure S2.** Time series of the SP-onset index and equatorial Pacific SSTs. (a) Time  
 66 series of the reversed SP-onset index (blue) and the equatorial eastern Pacific SST  
 67 (orange). (b) Time series of the SP-onset index (blue) and the equatorial central Pacific  
 68 SST (red).



69

70 **Figure S3.** Composite for El Niño and La Niña months when the EEP is cooler than  
 71 28°C. a-j, Evolution of SST, surface wind (first column), and 200hPa geopotential height  
 72 (second column) anomalies composited for the El Niño months in which the equatorial  
 73 eastern Pacific SST is less than 28°C at time lags of -3, 0, +3, +6, +9 months (lag time  
 74 shown in the lower left corner of the sub panels). k-t, As in a-j, but for La Niña months in  
 75 which the equatorial eastern Pacific SST is less than 28°C.

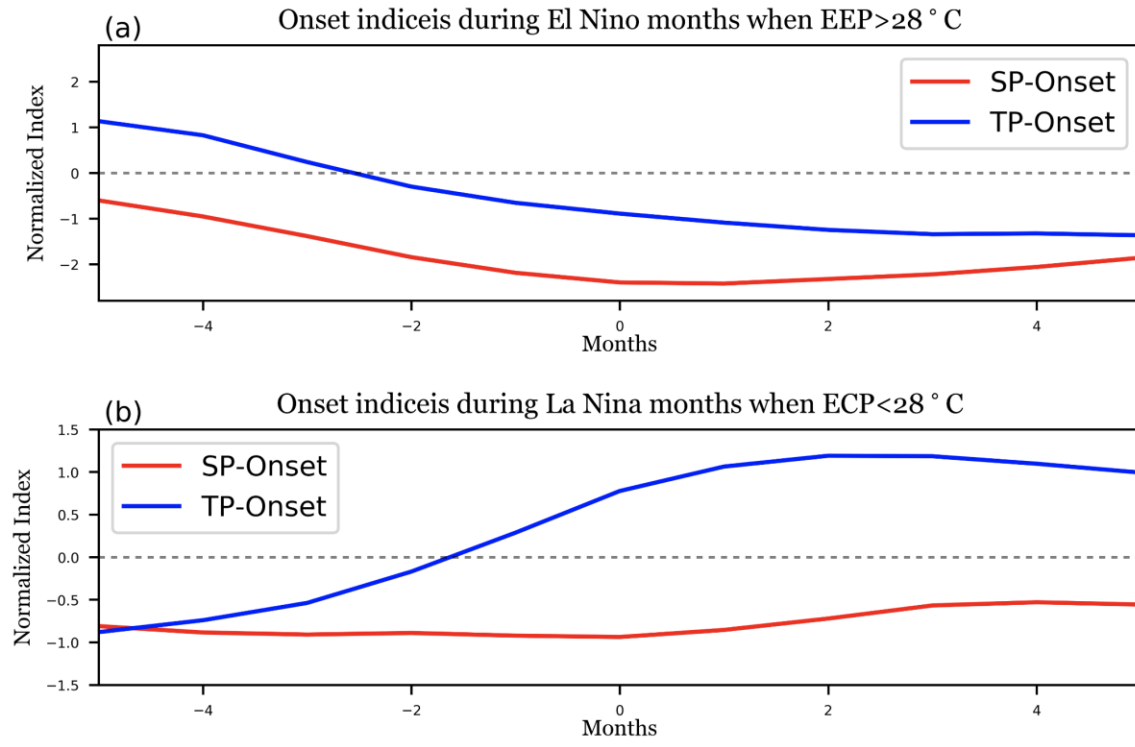
76



77

78 **Figure S4.** Composite of El Niño and La Niña months when the ECP is warmer than  
 79 28°C. As in Extended Data Figure 3 but for the El Niño and La Niña months when the  
 80 equatorial central Pacific is greater than 28°C, except the second and fourth panels are  
 81 plotted with the 850hPa geopotential heights over the 20°S–65°N.

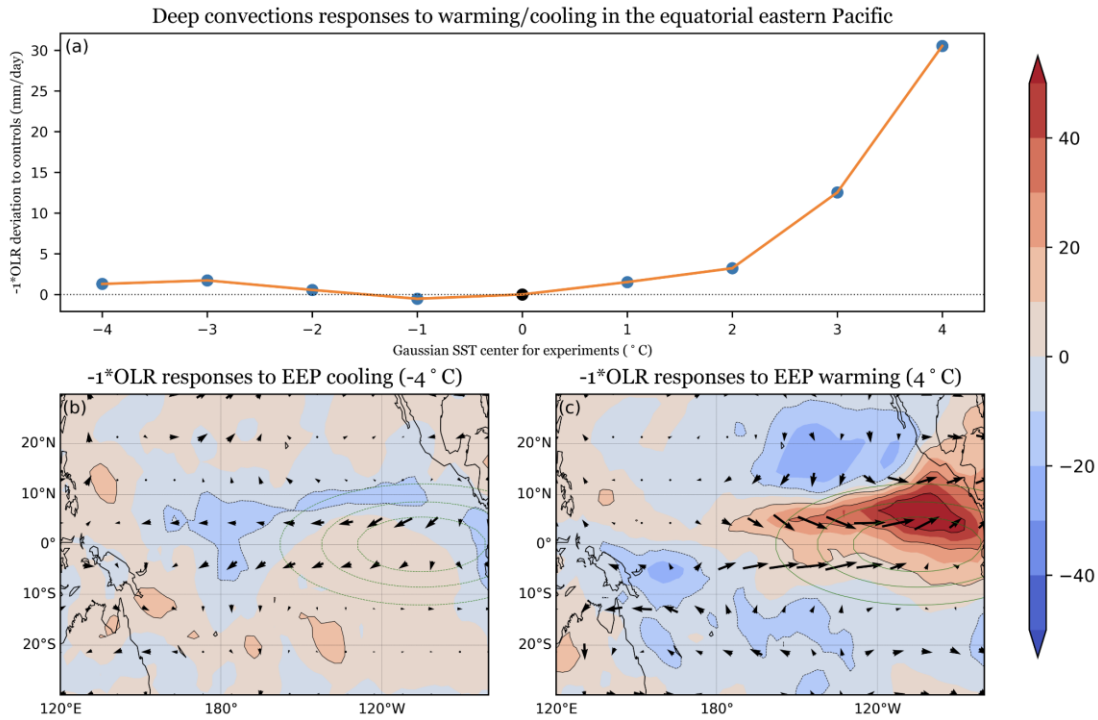
82



83

84 **Figure S5.** Evolutions of the TP-onset and the SP-onset indices composited during (a)  
 85 those El Niño months that have SSTs in the EEP that are above the deep convection  
 86 threshold (28°C) and (b) those La Niña months that have SSTs in the ECP that are below  
 87 the deep convection threshold. The “0” month in the figure marks the time when the local  
 88 SSTs in the EEP (ECP) first rise above (drop below) the 28°C threshold.

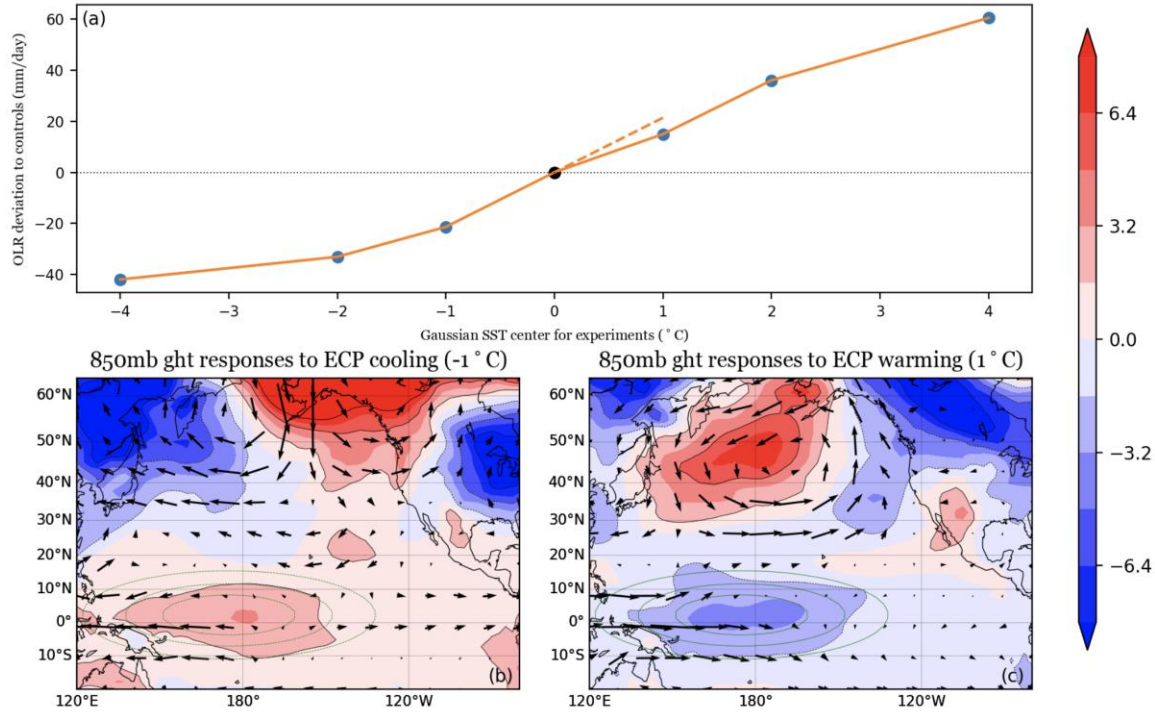
89



90 **Figure S6.** Atmospheric responses in model experiments with anomalous  
 91 warming/cooling in the equatorial eastern Pacific. a, Winter (DJF) Outgoing longwave  
 92 radiation ( $-1^*\text{OLR}$ ;  $\text{W/m}^2$ ) response (i.e., experiment values minus control simulation  
 93 values) in the 4-member ensemble experiments with  $-4, -3, -2, -1, +1, +2, +3, +4^{\circ}\text{C}$  of sea  
 94 surface temperature anomalies in the equatorial eastern Pacific. b,  $-1^*\text{OLR}$  (shading) and  
 95 850mb wind (arrows) responses in the  $-4^{\circ}\text{C}$  experiment. c, same as b, but for the  $+4^{\circ}\text{C}$   
 96 experiment. Green contours are the imposed warming/cooling at a  $1^{\circ}\text{C}$  interval.

97

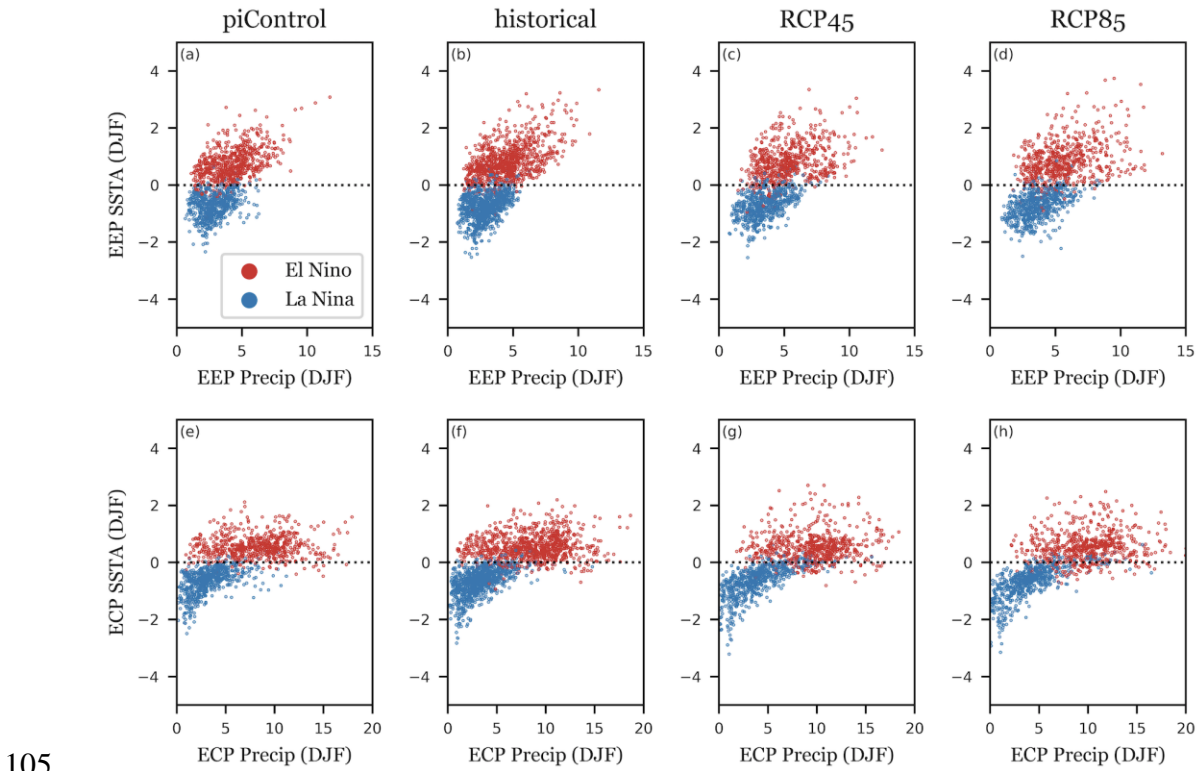
Deep convections responses to warming/cooling in the equatorial central Pacific



98

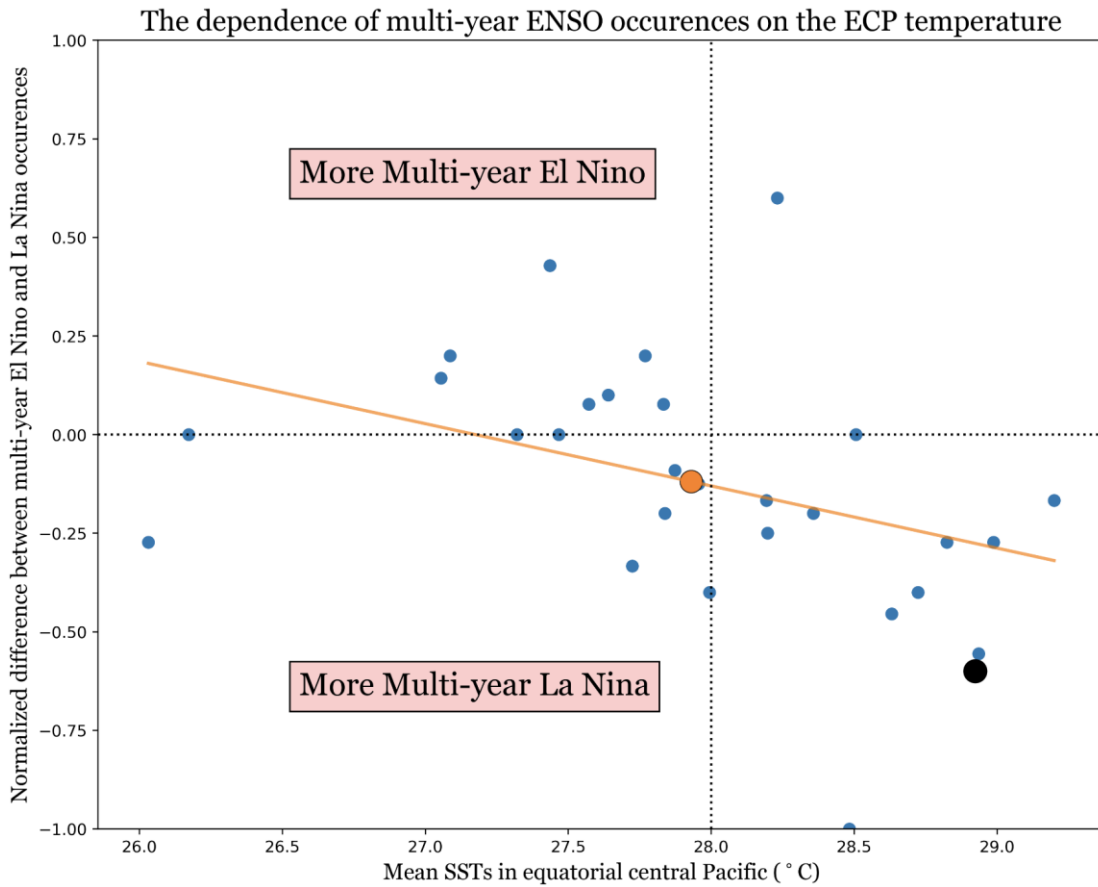
99 **Figure S7.** Atmospheric responses in model experiments with anomalous  
100 warming/cooling in the equatorial central Pacific. As in Figure 5, but with the SST  
101 anomalies imposed in the equatorial central Pacific experiments (centered at 0 $^{\circ}$ N and  
102 175 $^{\circ}$ E). b and c are the responses of 850mb geopotential heights in the -1 $^{\circ}$ C and +1 $^{\circ}$ C  
103 experiments, respectively. Green contours are the imposed warming/cooling at a 0.25 $^{\circ}$ C  
104 interval.

## Deep convection variations with SST anomalies



106 **Figure S8.** Relations between precipitation and SST anomalies in the EEP and ECP  
 107 regions. (a) The winter SST anomalies and precipitation in the EEP region for El Niño  
 108 (red) and La Niña (blue) events for the CMIP5 pre-industrial simulations (120 years). (b)  
 109 to (d) are for the historical (156 years), RCP4.5 (96 years during 2005-2100), and RCP8.5  
 110 (96 years during 2005-2100) simulations, respectively. (e) to (h) are for the ECP region.

111



112

113 **Figure S9.** The dependence of multi-year ENSO occurrences on the mean surface  
 114 temperature in the equatorial central Pacific. The y-axis is the difference between the  
 115 occurrences of multi-year El Niño and La Niña, which are normalized by the total  
 116 occurrences of the multi-year El Niño and La Niña in each CMIP5 pre-industrial  
 117 simulation. A multi-year event is identified by having a prior ENSO with same phase or  
 118 an ENSO event is longer than 18 months. The orange dot is the multi-model-mean of pre-  
 119 industrial simulations and the black dot is the reanalysis product. The orange line is their  
 120 linear fit.

121

122

<b>Model</b>	<b>Modeling Center</b>	<b>Model</b>	<b>Modeling Center</b>
ACCESS1-0	Commonwealth Scientific and Industrial Research Organization (CSIRO) and Bureau of Meteorology (BOM), Australia	GISS-E2-R-CC	NASA Goddard Institute for Space Studies
ACCESS1-3		HadGEM2-CC	Met Office Hadley Centre (additional HadGEM2-ES realizations contributed by Instituto Nacional de Pesquisas Espaciais)
bcc-csm1-1	Beijing Climate Center, China Meteorological Administration	HadGEM2-ES	
bcc-csm1-1-m		inmcm4	Institute for Numerical Mathematics
CanESM2	Canadian Centre for Climate Modelling and Analysis	IPSL-CM5A-LR	Institut Pierre-Simon Laplace
CCSM4	National Center for Atmospheric Research	IPSL-CM5A-MR	
CESM1-BGC	Community Earth System Model Contributors	IPSL-CM5B-LR	
CESM1-CAM5		MIROC-ESM	Japan Agency for Marine-Earth Science and Technology, Atmosphere and Ocean Research Institute (The University of Tokyo), and National Institute for Environmental Studies
CMCC-CM	Centro Euro-Mediterraneo per i Cambiamenti Climatici	MIROC-ESM-CHEM	
CMCC-CMS		MIROC5	Atmosphere and Ocean Research Institute (The University of Tokyo), National Institute for Environmental Studies, and Japan Agency for Marine-Earth Science and Technology
CNRM-CM5	Centre National de Recherches Météorologiques / Centre Européen de Recherche et Formation Avancée en Calcul Scientifique	MPI-ESM-LR	Max-Planck-Institut für Meteorologie (Max Planck Institute for Meteorology)
GFDL-ESM2G	NOAA Geophysical Fluid Dynamics Laboratory	MPI-ESM-MR	
GFDL-ESM2M		MRI-CGCM3	Meteorological Research Institute
GISS-E2-R	NASA Goddard Institute for Space Studies	NorESM1-M	Norwegian Climate Centre

124 **Table S1.** The names of the 28 CMIP5 models used in this study.